Paper pump for passive and programmable transport

Xiao Wang,[1] Joshua A. Hagen,[2] and Ian Papautsky[1,a)]
[1]*BioMicroSystems Laboratory, School of Electronic and Computing Systems, University of Cincinnati, Cincinnati, Ohio 45221, USA*
[2]*Air Force Research Laboratory, 711th Human Performance Wing, Wright-Patterson Air Force Base, Dayton, Ohio 45433, USA*

(Received 1 November 2012; accepted 25 January 2013; published online 6 February 2013)

In microfluidic systems, a pump for fluid-driving is often necessary. To keep the size of microfluidic systems small, a pump that is small in size, light-weight and needs no external power source is advantageous. In this work, we present a passive, simple, ultra-low-cost, and easily controlled pumping method based on capillary action of paper that pumps fluid through conventional polymer-based microfluidic channels with steady flow rate. By using inexpensive cutting tools, paper can be shaped and placed at the outlet port of a conventional microfluidic channel, providing a wide range of pumping rates. A theoretical model was developed to describe the pumping mechanism and aid in the design of paper pumps. As we show, paper pumps can provide steady flow rates from 0.3 μl/s to 1.7 μl/s and can be cascaded to achieve programmable flow-rate tuning during the pumping process. We also successfully demonstrate transport of the most common biofluids (urine, serum, and blood). With these capabilities, the paper pump has the potential to become a powerful fluid-driving approach that will benefit the fielding of microfluidic systems for point-of-care applications. © *2013 American Institute of Physics*.
[http://dx.doi.org/10.1063/1.4790819]

I. INTRODUCTION

Micropumps are critical components of integrated microfluidic systems. Such pumps must provide steady flow, easy adjustment of flow rate, rapid transport, and minimal dead volume. A wide range of pumping methods have already been reported.[1–5] While active on-chip pumping methods, such as those using electric field in electroosmotic[1] or electrowetting-on-dielectric,[3] are capable of rapid transport of small sample volume, their complexity coupled with power requirements and the often-complex control circuitry is undesirable for point-of-care (POC) applications.

As an alternative to active pumping, a number of passive pumping methods that rely only on the microchannel geometry have been reported over the years, bringing significant simplification to pumping and improving portability of microfluidic devices.[6–10] For instance, differences in surface tension can be exploited to pump sample from a droplet at the inlet port to a larger droplet on the outlet port through a microfluidic channel.[6] Differences in capillarity can be created by dry-etching silicon microstructures with different shapes and arrangements,[7] while evaporation can be used to create pressure differences between reservoirs to enable transport.[8] Using the innate high air solubility and porosity of PDMS (polydimethylsiloxane), degas-driven pumping has also been reported.[9,10] While these passive pumping methods are elegant, a shortcoming that all of them share is that pumping mechanism must be fully integrated with microfluidic channel;[7–10] and once the device is fabricated the flow rate cannot be adjusted easily.

Liquid can transport passively in porous media (e.g., paper). The passive transport is driven by capillary force which is generated by curvature at the air-liquid interface.[11] The

a)Author to whom correspondence should be addressed. Electronic mail: ian.papautsky@uc.edu. Tel.: (513) 556-2347.

capillary-based transport of liquid in paper of various shapes has been investigated in recent decades, including rectangular,[12,13] circular,[14–16] triangular,[17] rectangular combined with fan shape,[18] and other two-dimensional paper networks.[19] Based on the capillary-based passive sample transport in paper, paper microfluidics has been brought up recently and gained substantial interest due to the ultra-low cost, simple fabrication, passive transport with numerous applications already demonstrated.[20–29] Compared with the conventional polymer-based devices, sample transport in paper devices only depends on capillarity of the paper, thus avoiding additional pumping systems. Nevertheless, despite the numerous advantages, paper microfluidics still suffers from the difficulties in transporting cells in the paper matrix[30] and decrease effectiveness of paper assays due to biosample interaction with cellulose fibers.[24]

In this work, we integrate circular/sector-shape paper with conventional PDMS microfluidics as a capillarity-based pump (Fig. 1) in order to take advantage of paper as a lightweight, disposable and programmable pump without sacrificing the advantages of well-developed polymer-based microfluidics. A theoretical model was developed to guide design of the paper pump for steady flow rate and programmable multi-stage pumping. Since the paper pump is not monolithically integrated with the microfluidic system, it is easy to replace the pump according to different flow-rate requirements. The described pumping approach combines the advantages of paper fluid transport and polymer channel functionally into a simple lab-on-a-chip (LOC) platform. Such integration has a potential to increase portability of LOC systems as well as lowering the cost tremendously from the aspect of fluid-driven system.

II. MATERIALS AND FABRICATION

Construction of paper pumps and their integration with microfluidic channels involves a sequence of simple fabrication steps. We cut paper pumps from Whatman No. 1 (180 μm thick) or No. 4 (210 μm thick) filter paper. The paper can be cut to shape with a wide range of methods, from low-tech scissors and knives to high-tech xurography and laser cutting.[31] The typical resolution of the scissors or knife approaches 500 μm; while attractive due to simplicity and cost, it is not practical due to low resolution and poor reproducibility, which lead to poor control of pump flow rate. Alternatively, xurography using a knife plotter or laser cutting offer excellent resolution (<5 μm) and reproducibility but are costly. We used a digital craft cutter (Quickutz Silhouette SD), which offers a mid-range blend of characteristics including good resolution (~50 μm), ease of use, and relatively low cost (<$200).

Microchannels (20 mm × 1 mm × 50 μm, $L \times W \times H$) were fabricated in PDMS by conventional soft lithography. While using SU-8 masters is the most common approach to generate

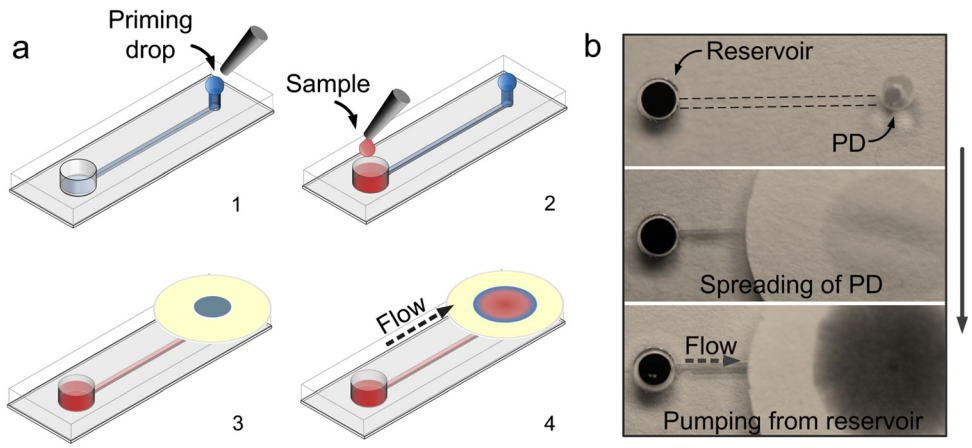

FIG. 1. (a) Operation of the paper pump for pumping fluid through a microfluidic channel: (1) channel priming, (2) sample introduction, (3) initial spreading of the priming drop, and (4) sample pumping. (b) Sequence of time lapse images illustrating operation of paper pump (PD = priming drop).

microfluidic channels in PDMS, we used a tape master.[32] For this, 3 M tape was first attached to a plastic carrier sheet (Silhouette America) and cut into the designed shape by the craft cutter, and then transferred from the carrier and to the surface of a Petri-dish. This method provides a fast and low-cost way to make simple masters with dimensions larger than 250 μm. The quality of the tape master reduced severely below 250 μm because of the resolution limitations of the craft cutter. Next, the tape masters were degassed for 30 min to remove any bubbles trapped under the tape. PDMS was cast and cured at 60 °C for 2.5 h to avoid damaging the tape master. Inlet reservoirs and outlet ports were cored with a 3 mm diameter punch and a 14 gauge dispensing tip, respectively. The PDMS mold was bonded to a standard microscope glass slide (75 mm × 25 mm) to seal the channel using a plasma surface treater (BD-20AC, Electo-Technic Products, Inc.).

III. THEORETICAL MODEL OF PAPER PUMPING

To understand the mechanism of paper pumping through a PDMS microchannel and help design optimal parameters of the paper pump, we developed a theoretical model. Using a thin radial capillary to model capillary action of paper, we calculate the volumetric change of liquid inside the paper which leads to the pumping rate (Q) in the microchannel. The overall structure of the wetted surface is shown in Fig. 2(a) which consists of three parts: an inlet reservoir, a microchannel and an outlet port with paper pump.

To predict the motion of liquid inside the paper pump, we first estimate hydrodynamic pressure at the output. This is determined by considering the capillary action in the paper, which is modeled as a thin radial capillary of equivalent thickness h_{eq} (Fig. 2(b)). Then, the pressure drop is described as a function of capillary diameter and the wicking radius r[14,15] as

$$P_2 - P_3 = \frac{12\mu r}{h_{eq}} \ln\left(\frac{2r}{b}\right)\frac{dr}{dt} \quad , \tag{1}$$

where P_2 is the pressure at the outlet port, P_3 is the capillary pressure in the radial capillary, b is the diameter of the outlet port, and μ is the dynamic viscosity of fluid (0.001 Pa•s for our case of colored water at room temperature). This equation takes into account the thickness of the radial capillary (h_{eq}) and the size of the output port ($b = 1.2$ mm), which both influence the area wetted by the sample.

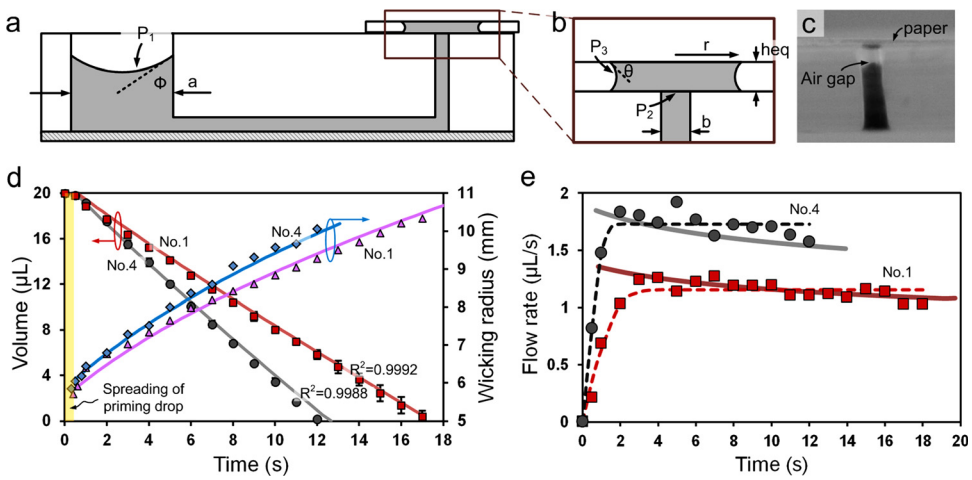

FIG. 2. (a) Theoretical model of fluid pumping from inlet reservoir through microfluidic channel with a paper pump. (b) Paper can be treated as a thin radial capillary with equivalent thickness h_{eq}. (c) The side view of outlet port in no-priming drop situation is shown. (d) Measurements were carried out on both the volume change in inlet reservoir and wicking radius of the paper on the outlet port. Filled symbols demonstrate experimental data; solid lines represent theoretical results. (e) Measurement of flow rate as a function of time. Filled symbols show experimental data; solid lines represent theoretical results.

Examining the PDMS microchannel as a whole, we can determine that the outlet port pressure P_2 based on the pressure drop along the microchannel (ΔP) as $P_2 = P_1 - \Delta P$. The total pressure P_1 equals the sum of ambient pressure (P_0) and Laplace pressure[33] within the fluid sample inside the inlet reservoir. P_1 is calculated to be nearly the atmospheric pressure P_0.[32] The pressure drop ΔP can be determined from the flow rate (Q) in the microchannel and the fluidic resistance (R) of the microchannel. The pressure drop ΔP in the PDMS microchannel in our experiment is calculated to be 3.8 kPa.[32] Thus, compared to P_1, ΔP is much smaller, leading to P_2 being approximated as P_0.

Next, we examine pressure P_3 in the paper, which is approximated as a radial capillary. By considering the vertical (r_V) and horizontal (r_H) principal radii of curvature, the capillary pressure P_3 is determined from the Young-Laplace equation as[32]

$$P_3 = P_0 - \gamma\left(\frac{1}{r} - \frac{2\cos\theta}{h_{eq}}\right). \tag{2}$$

Having arrived to expressions for both P_2 and P_3, we can now return to Eq. (1) in order to arrive to a relationship between the wicking radius (r) and time (t). This is accomplished by substituting expressions for P_2 and P_3 back into Eq. (1), yielding an expression that describes the rate of change in the wetting radius

$$\gamma\left(\frac{1}{r} - \frac{2\cos\theta}{h_{eq}}\right) = \frac{12\mu r}{h_{eq}} \ln\left(\frac{2r}{b}\right)\frac{dr}{dt}\ . \tag{3}$$

Integrating Eq. (3) leads to the description of capillary action inside the paper pump:

$$\left(\frac{2r}{b}\right)^2\left[ln\left(\frac{2r}{b}\right)^2 + \left(\frac{b}{2r}\right)^2 - 1\right] = \frac{8\gamma h_{eq}\cos\theta}{3\mu b^2}t. \tag{4}$$

One remaining unknown term in the above equation preventing us from calculating wicking radius is the wetting angle (θ) between the liquid sample and the cellulose fibers in the paper. While this information is not available from the manufacturer, earlier work by Borhan and coworkers[34] has estimated the term $h_{eq}\cos\theta$ to be $\sim$0.5 μm for water in No. 1 filter paper ($h_{No1} = 180\ \mu$m). Since both No. 1 and No. 4 paper are manufactured from the same material, the same contact angle is expected and can be used in calculations for both types of paper. Thus $h_{eq}\cos\theta$ term for No. 4 filter paper can be estimated as $\sim$0.58 μm considering the paper thickness ($h_{No4} = 210\ \mu$m).

To accurately predict the flow rate Q of the paper pump, we must account for the moisture content in the paper. For this, we must combine Eq. (4) with an average volumetric moisture content K which determines the wetting area A. We can define the moisture content K as $K = dV_{ab}/dAh$ where h is the thickness of paper and V_{ab} is the absorbed volume. We can determine K experimentally by recording the wetting area dA on the paper after absorbing liquid sample of a known volume dV_{ab}. K is calculated to be 0.47 for No. 1 filter paper and 0.48 for No. 4 filter paper.

Assuming uniform, circular wicking front, we can now express change in volume per unit time as $dV/dt = 2\pi r dr/dt$. Combining the thickness of paper and moisture content, the flow rate Q can now be described as

$$Q = \frac{dV}{dt} = 2\pi K h r\frac{dr}{dt}. \tag{5}$$

Simplifying further to eliminate dr/dt using Eq. (4), the volumetric flow rate can be predicted by

$$Q = \frac{2\pi K h\gamma h_{eq}\cos\theta}{3\mu\ln\left(\frac{2r}{b}\right)^2}. \tag{6}$$

We must note that although dr/dt appears in Eq. (3), the resulting expression cannot be used to calculate flow rate as values of the radial capillary equivalent thickness h_{eq} and the wetting angle θ between the liquid sample and the cellulose fibers are not known. The flow rate can, however, be calculated using Eq. (6) since the product term $h_{eq}\cos\theta$ was estimated by Borhan and coworkers,[34] as we discuss above.

In this analysis, we derive expressions necessary to calculate the flow rate inside the microchannel driven by a paper pump. Using this theoretical model, we can now predict the rate of flow in the microchannel based on the shape of the paper pump and the progression of the wetting radius, which is easily observed (and imaged) from overhead. The expression also suggests a number of variables that can be used to modify the flow rate. For example, increasing thickness of the paper h will lead to the flow rate enhancement. We should note, however, that if the paper thickness increased too much (e.g., >1 mm), spreading of the liquid sample leads two-dimensional motion involving both radial and vertical wicking. This would lead to inaccuracies in the calculation using this thin radial capillary model which does not account for vertical wicking. The flow rate is also influenced by the geometry of the microchannel outlet port b, the properties of the liquid to be transported (viscosity μ and surface tension γ), and the properties of the paper (thickness h and the wetting contact angle θ). In addition, different types of paper have different capacity for storing water due to their porosity, thus leading to different volumetric moisture content K, which directly affects the transport rate. Thus, we developed a theoretical model based on a thin radial capillary that describes the capillary action in a circular paper pump and predicts the flow rate generated by the pump. The further experimental verification of the model will be demonstrated in the experimental section below.

IV. EXPERIMENTAL RESULTS

A. Characterization of paper pump

In the first set of experiments, we demonstrated pumping by transporting water through a straight PDMS microchannel (Fig. 1). The empty microchannel was first primed with water by injection from the outlet port. A 20 μl liquid sample was then added to the inlet reservoir (3 mm diameter). Before placing a paper pump at the outlet port, an additional priming drop was dispensed at the outlet to trigger the pumping process. Priming is critical to initiate wicking and thus pumping. Without priming, an air gap forms immediately after the paper absorbs a very small volume of liquid at the outlet port which inhibits further pulling (Fig. 2(c)). This is evident from the model, which shows that to ensure continuous pumping $P_2 > P_3$ must be satisfied through the entire pumping process, leading to $r > h_{eq}/2\gamma\cos\theta$. It implies that the initial wicking radius must be larger than $h_{eq}/2\gamma\cos\theta$ before the pumping process starts. Once a paper pump is placed at the outlet port, priming takes place in less than 0.5 s followed by the pumping process from the inlet reservoir towards outlet paper pump. For the initial experiments, the area of paper pump was large and sample volume was kept small (20 μl) so that liquid samples did not wet the entire area.

First illustrated are the results from measurements of wicking radius on paper and the volume change in the liquid in reservoir. Wetted areas were measured in ImageJ® from overhead images, and the average wicking radii were calculated. To measure volume changes, inlet reservoirs were imaged from side using a high resolution camera with a macrolens (Canon EOS Rebel T3i with EF 100 mm f/2.8 L Macro IS USM Lens). Details of these measurements and sample images are presented in supplementary information.[32] Again, we used ImageJ® to analyze side images and videos. A 0.5% pigment dispersion of food dye was used to aid visualization.

From our observations, the pumping process can be partitioned into two stages. In the first stage, the priming stage, the priming drop spreads in ~0.5 s (indicated by yellow shading Fig. 2(d)). Next, continuous pumping from the reservoir begins, represented by the time-dependent increase in the wicking radius. For instance, spreading of the priming drop led to an initial wicking radius of $r_{No1} = 6$ mm for the No. 1 filter paper, followed by an increase to 10.7 mm

during pumping of a 20 μl sample over the 18 s period. Consider that the priming drop creates an initial wet area, the theoretical calculation of r vs. t starts from $r = 6$ mm using on Eq. (4). The calculated results are in a strong agreement with experimental results. From these results, we conclude that our theoretical model describes the second-stage wicking accurately. Both experimental and theoretical results illustrate that wicking radius of No. 4 filter paper increased faster than that of No. 1 filter paper. This is expected due to differences in thickness and filtration speed of these two paper types. More specifically, Whatman No. 4 filter paper ($h_{No4} = 210\ \mu$m) is thicker than the No. 1 paper ($h_{No1} = 180\ \mu$m) and has a larger filtration speed (150 s) than No. 1 filter paper (37 s). These two factors lead to a faster wicking in the paper pump made of No. 4 filter paper. Volume of sample left in the inlet reservoir was measured and also plotted in Fig. 2(d) for No. 1 (red square) for No. 4 (grey circle). In both cases, the 20 μl volume depleted linearly in less than 20 s. It indicated that the flow rate generated by the paper pumping was very stable. The theoretical prediction of volume change was also presented (Fig. 2(d)) which was obtained from integration of theoretical plot of flow rate (Fig. 2(e)).

The flow rate increased in the first 2 s due to the spreading of priming drop, after which pumping process began and the flow rate entered steady state (Fig. 2(e)). For No. 1 filter paper, the average flow rate during the steady state was 1.15 $\pm$ 0.08 μl/s, which is in strong agreement with the theoretical prediction using Eq. (6). Note that the calculation of flow rate starts from $r = 6$ mm due to the initial wetting area generated by the priming drop. In the case of No. 4 filter paper, the results of experiment and calculation were also very close: 1.7 $\pm$ 0.1 μl/s and 1.6 $\pm$ 0.08 μl/s, respectively. The small standard deviation illustrates that the flow rate provided by paper pumping is steady after an initial priming period of < 2 s. To put this in a prospective, the same flow rates can be obtained with a commercial syringe pump and a 3 cc or 5 cc syringe, although accuracy of these commercial syringe pumps[35] is greater ($<1\%$ variation vs. $\sim 5\%$ for the paper pump). The $\sim 5\%$ variation comes from the nature of capillary flow in paper pump where the flow rate decays by time during the pumping process which is shown both in theoretical calculation and experimental results (Fig. 2(e)). In terms of the reproducibility of the pump, we tested three individual pumping processes using Whatman No. 1 and No. 4 papers showing reproducibility of 3% and 2.5% correspondingly, which cannot compete with the commercial syringe pumps (0.05%).[35] The reproducibility issue might be caused by the material feature of paper. As a porous media made of cellulose, paper is not uniform with respect to the pore size and pore density. The variability of paper influences capillary flow leading to the deviation of flow rate between each pumping process. Besides, the reproducibility can also be affected by the variation of the priming drop volume induced by the pipette.[36]

B. Flow rate control

The flow rate of the paper pump can be tuned by simply changing pump shape to a sector of different angles (Fig. 3(a)). Theoretically, for both sector-shaped and circular paper pump, the two principal radii of curvatures ($r_V = h_{eq}/2\gamma\cos\theta$ and $r_H = r$) in the radial capillary model should be the same which leads to the same capillary pressure. Thus, the relationship between the wicking radius r and time t should remain the same for the sector-shape pumps. As a result, the volume of liquid absorbed by the paper per unit time should be linearly related to the angle of sector-shape leading to the correlation between the flow rate and the angle. To test the hypothesis that angle of a sector-shaped pump is linearly correlated with the flow rate, we fabricated pumps with angles of 30° to 360° in both No. 1 and No. 4 filter paper. Our experimental results, presented in Fig. 3(b), show that indeed the pump flow rate depends linearly on the sector angle. The flow rates increased from 0.3 μl/s (30°) to 1.14 μl/s (360°) for No. 1 filter paper, and from 0.57 μl/s to 1.71 μl/s for No. 4 filter paper. From these results, we can arrive to an empirical equation that describes the relation between angles of the sector shape and the pump flow rate:

$$Q = \frac{1}{\pi}\begin{bmatrix} 0.89 \\ 1.03 \end{bmatrix}\alpha + \begin{bmatrix} 0.27 \\ 0.67 \end{bmatrix}, \tag{7}$$

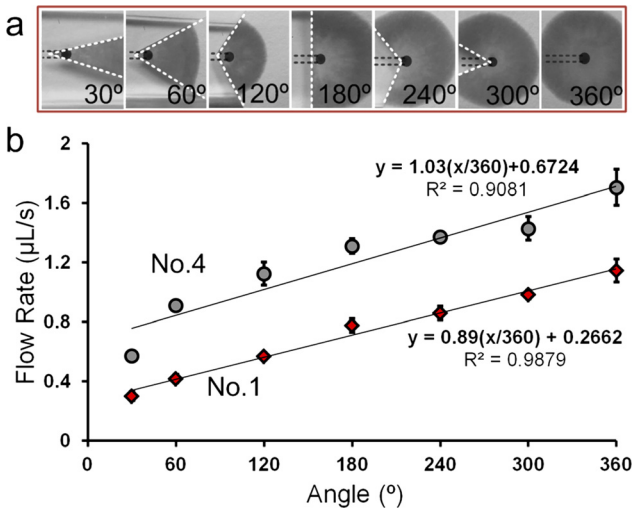

FIG. 3. Flow rate can be adjusted through using sector-shaped paper with different angles. (a) Grey-scale images show pumping with sector-shaped paper pumps of 30° to 360°. (b) The angle and flow rate exhibit a linear relationship for both Whatman No. 1 and No. 4 filter papers. Experimental data are shown with filled symbols.

where α is the angle of sector-shaped pump. Equation (7) can serve as the guide in designing a paper pump to achieve different flow rates. Note that in these equations, when α reduces to 0°, the flow rate still has a finite positive value ($Q > 0$), which seems to contradict the theoretical predication that the flow rate should be 0 μl/s with 0° sector-shaped paper pump. However, considering the fact that the microchannel output has a finite diameter and a priming drop must be used to initiate the pumping action, a finite rate at infinitely small sector is reasonable. For the same volume of the priming drop, the initial wicking radius immediately following the complete spreading is different for sector pumps of different angle. For example, the initial wicking radius is smaller in a circular pump than that of a 30° sector-shaped pump. This initial radius has an influence on the original state of capillary pressure P_3, leading to deviation from the theoretical predictions. Therefore, the linear relationship between flow rate and angle is practical for angles > 30°.

From our experiments, sector-shaped paper pumps made of Whatman No. 1 and No. 4 paper with different angles could provide flow rate with a range from 0.3 μl/s to 2 μl/s. The paper pump generates flow rate in μl/s range which is much higher than several other passive pumps. For example, evaporation-based pumping could provide flow rate of μl/h;[8] degasing-driven pump could transport samples with flow rate of nl/s.[9] However, in terms of the flow rate range, paper pump cannot compete with commercial syringe pumps which typically offer flow rate ranging from ~1 pl/min to ~100 ml/min.[37]

C. Programmable pumping

Sector shapes can be cascaded to create a single pump to achieve automatic flow-rate adjustment during the pumping process. A paper pump with geometry of a circular shape leading to 30° sector-shape is shown in Fig. 4(a). The pumping process contains two steady phases connected by a transition period. In phase 1, the pumping behavior, as a circular, with a flow rate of 1.14 μl/s (Fig. 4(b)). When the front of the fluid spreads and covers the entire area of the circular region, the flow rate begins to transition, decreasing slowly (Fig. 4(b), black arrows). The slow decrease is caused by further wetting in circular region. When the circular region is fully saturated, the pumping process enters the steady phase 2 (Fig. 4(b), red arrows) in which the flow rate is maintained at 0.3 μl/s. By varying the diameter of the phase 1 circular region from 11 mm to 17 mm, the corresponding duration of the phase 1 varies from 5 s to14 s. The transition period of 10 s to 16 s for each group with increasing diameters is reasonable

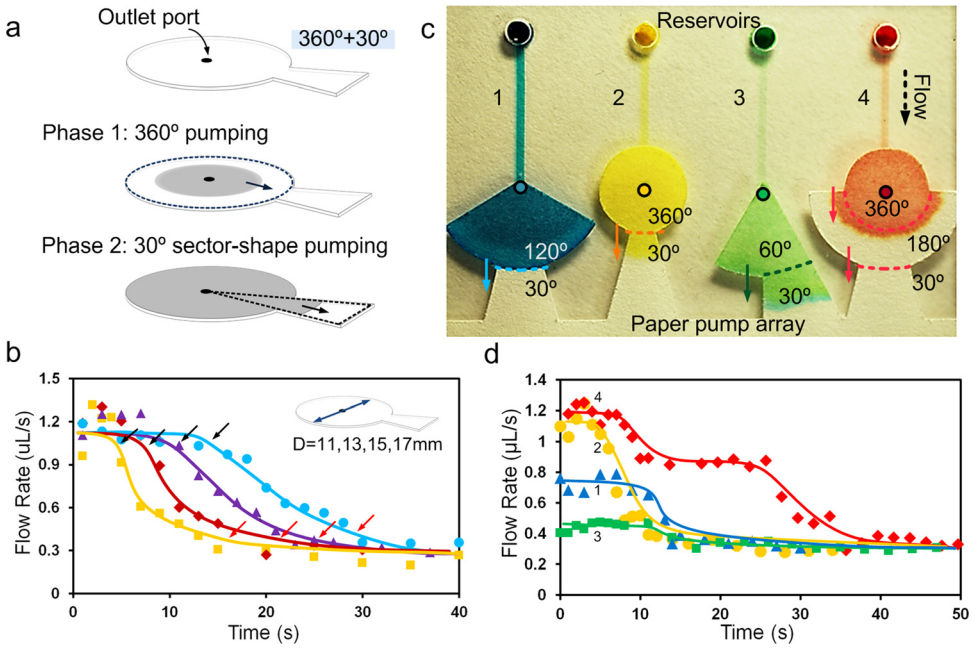

FIG. 4. (a) Programmable paper pump with transition from 360° to 30°. (b) The pumping process includes two steady phases. The dots represent the experimental results for different diameters ($D_{yellow} = 11$ mm, $D_{red} = 13$ mm, $D_{purple} = 15$ mm, $D_{blue} = 17$ mm) and solid lines are the corresponding trendlines. (c) An array of four different paper pumps transporting dyed water through a microfluidic channel array with two-phase or three-phase pumping. (d) Programmable flow rate tuning of the pump array. Numbers match the flow performance to the pump number in (c).

because longer time is required to saturate the whole area of a circular region with a larger diameter.

Several paper pumps that offer different automatically adjustable flow rates can be integrated into an array by simply using a craft-cutter (Fig. 4(c)). Fluids were pumped through an array of four microfluidic channels by the pump array. The automatic modifications of flow rates for each channel are plotted in Fig. 4(d). For channels 1, 2 and 3, pumps (120°→30°, 360°→30°, and 60°→30°) provided different flow rates in two pumping phases (0.67 μl/s →0.34 μl/s, 1.17 μl/s→0.34 μl/s, 0.43 μl/s→0.34 μl/s, correspondingly). For channel 4, the paper pump was created by combining three shapes (360°→180°→30°) to create three stages (1.17 l/s →0.85 μl/s→0.34 μl/s). A sector-shaped paper using that transition from a small angle (30°) to a larger angle (180°) was also tested in an attempt to increase the pump rate. However, in this design, the first stage proved to be limiting and the flow rate remained steady instead of increasing. The integration of paper pump array implies the simplicity and flexibility of flow rate adjustment of paper pump and also shows the possibility of pulling samples from complex LOC systems with multiple channels using a single paper pump.

Compared to other passive pumping methods,[6–10,38] the paper pump presented in this work exhibits programmable pumping functionality that can achieve controlled multi-stage pumping from high to low flow rate. However, compared to the programmable function of commercial syringe pump, paper pump has certain limitations in terms of long transition time (~10 s for paper pump vs. 5 ms transition for syringe pump)[39] and single direction flow rate modulation (from high to low flow rate).

D. Transport of biological samples

Three biological samples (urine, diluted blood, and serum) that are widely used in POC diagnostic systems were used to test the feasibility of the paper pump. Our experimental results show that all these samples were successfully transported, without clogging, through a microchannel (Fig. 5). We also attempted transport of whole blood but were not successful as the

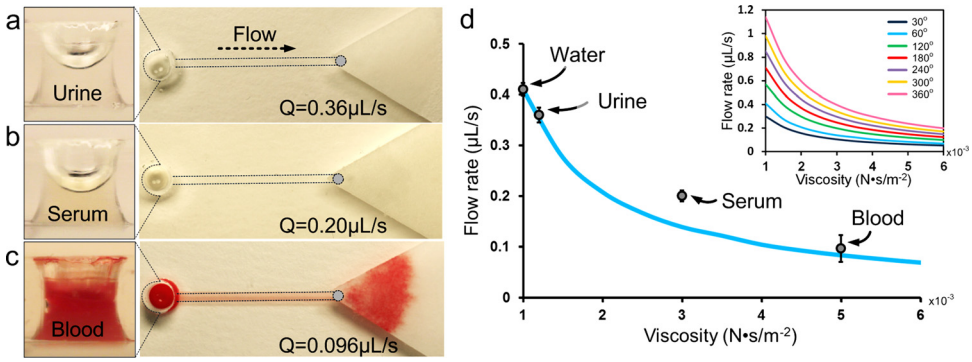

FIG. 5. Pumping of (a) urine, (b) bovine serum, (c) human blood (1× dilution) with 60° sector pumps. (d) Relationship between flow rate and viscosity for the 60° sector pump obtained from the theoretical model (blue line) and experimental data (grey circles). Three individual experiments were carried out for each of the samples. Inset illustrates the relationship between flow rate and viscosity of the sample from the theoretical model for various sector pumps.

microchannel was clogged by the blood cells which stopped the flow. The flow rate of transport was found to vary from sample to sample, as a function of viscosity. Urine, which is mostly water and has a viscosity of 1.1 mPa·s[40] at room temperature, exhibited the highest rate of transport, close to that of water. Blood serum, which is devoid of cell matter but contains protein, is more viscous (3 mPa·s)[41] and exhibited a slower rate of transport, as expected. Blood is a non-Newtonian fluid,[42] whose viscosity is dependent on the shear rate and hematocrit value. For the 1× dilution used in this work, viscosity is approximately 5 mPa·s.[43] While the pumping flow rate decreases with sample viscosity, as expected, the relationship is not linear. Nevertheless, it can be predicted using Eqs. (4) and (6) by inserting the different viscosity values and calculating the corresponding flow rate (Fig. 5(d) inset). The experimental results of biofluids pulling with 60° pump match the theoretical trend well (Fig. 5(d)), illustrating that the paper pump can be used for transport of real-world biological samples.

V. CONCLUSIONS

We presented an ultra-low-cost, passive pump based on capillary-action in paper that can be integrated with conventional microfluidic systems to efficiently drive fluid with a stable and tunable flow rate. The polymer-paper hybrid system takes advantage of the well-developed polymer microfluidics and paper to drive fluid through it. The approach provides a valuable method for constructing low-cost, portable microfluidic devices. Similar concepts have been put forward recently by others. Xu *et al.*[44] inserted a plug of filter paper into the outlet of a microfluidic chip to serve as a capillary-evaporation based pump. The paper plug produced respectable flow rates, in the μl/min range. Wang *et al.*[45] integrated filter paper at the end of a microchannel for fluid-driving, which also yielded flow rates in the μl/min range. While both paper-based pumps were used to fulfill sample delivery for DNA assay[44] and one-step protein detection[45] in polymer-based microchannels, neither had a straightforward approach to control flow rate nor a comprehensive analysis of the pumping mechanism. We developed a theoretical model of paper pump that describes the pumping mechanism in detail. The paper pump could achieve a stable flow rate in the μl/s range that is much higher than previous ones with a much simpler way to control the flow rate.

Compared with other types of passive pumping approaches like surface-tension-based passive pump,[6] the paper pump provides one-time transport with constant flow rate of relatively large volume of sample ($20\,\mu l \sim 40\,\mu l$ in our experiments) through a microchannel without refilling. Compared to the "on-chip" capillary pump,[7] coupled capillary/evaporation pump[8] and degas-driven pump[9,10] in which pump units were fully connected with microfluidic systems, paper pumping offers a straightforward method to adjust the flow rate for different requirement—simply use a new piece of pump with specific geometry. Compared to hand-powered membrane

pump[38] which enables transporting large sample volume (~240 μl) with high flow rate (~125 μl/min), paper pump provides comparable sample throughput (~2 μl/s) with a much simpler fabrication process. Besides, the flow rate is much more constant than the membrane pump in which the flow rate drops from 125 μl/min to 25 μl/min during the first 3 min. Further, when cut into simple cascaded geometries, paper pumps can provide the function of programmable flow rate tuning which is difficult to achieve in a passive system and has not been demonstrated previously.

While we successfully demonstrated the use of paper for passive pumping, a number of challenges still remain. The highest flow rate it can provide is ~2 μl/s, which may limit its applications. Besides, paper pump cannot achieve programmable modulation of flow rate from low to high during the pulling process due to the limitation of the geometry. Moreover, the area of the pump site remains in centimeter-scale and maybe too large for some microfluidic systems. This might be overcome by elongating channel near the outlet port to create a specific area to accommodate the paper pump or by decreasing the area of paper (and thus pumped sample volume) or by folding/rolling paper into a smaller area. By overcoming these remaining challenges, we can envision the tremendous potential of this paper based pumping approach integration with microfluidic systems for simple and inexpensive pumping. For example, it can be used for providing reagents for assays through microfluidic channels, for supplying buffers for cell culture, lysis through microfluidic devices, etc. Additionally, the paper pumps can be easily discarded and replaced with a new pump for extended use of POC devices. Furthermore, microfluidic devices can be made into arrays, primed automatically using automated liquid handling robots[46] and combined with designed paper pump arrays to achieve automated, high-throughput fluidic transport. As a passive pumping method, the paper pump is a promising candidate that could motivate the simplification of applied benchtop microfluidics from the aspect of fluid-driving approach and benefit the development of the promising POC systems.

ACKNOWLEDGMENTS

This work was supported by funds provided by the Air Force Office of Scientific Research and by the Human Effectiveness Directorate, 711 Human Performance Wing, Air Force Research Laboratory.

[1]D. J. Laser and J. G. Santiago, J. Micromech. Microeng. **14**, 35 (2004).
[2]C.-C. Hong, J.-W. Choi, and C. H. Ahn, J. Micromech. Microeng. **17**, 410 (2007).
[3]R. B. Fair, Microfluid Nanofluid **3**, 245 (2007).
[4]S. M. Langelier, D. S. Chang, R. I. Zeitoun, and M. A. Burns, Proc. Natl. Acad. Sci. U.S.A. **106**, 12617 (2009).
[5]R. Gorkin, J. Park, J. Siegrist, M. Amasia, B. S. Lee, J. Park, J. Kim, H. Kim, M. Madou, and Y. Cho, Lab Chip **10**, 1758 (2010).
[6]G. M. Walker and D. J. Beebe, Lab Chip **2**, 131 (2002).
[7]M. Zimmermann, H. Schmid, P. Hunziker, and E. Delamarche, Lab Chip **7**, 119 (2007).
[8]N. S. Lynn and D. S. Dandy, Lab Chip **9**, 3422 (2009).
[9]D. Y. Liang, A. M. Tentori, I. K. Dimov, and L. P. Lee, Biomicrofluidics **5**, 024108 (2011).
[10]I. K. Dimov, L. Basabe-Desmonts, J. L. Garcia-Cordero, B. M. Ross, A. J. Ricco, and L. P. Lee, Lab Chip **11**, 845 (2011).
[11]L. A. Richards, J. Appl. Phys. **1**, 318 (1931).
[12]T. Gillespie, J. Colloid Sci. **14**, 123 (1959).
[13]H. Fujita, J. Phys. Chem. **56**, 625 (1952).
[14]A. Marmur, J. Colloid Interface Sci. **124**, 301 (1988).
[15]D. Danino and A. Marmur, J. Colloid Interface Sci. **166**, 245 (1994).
[16]M. Conrath, N. Fries, M. Zhang, and M. E. Dreyer, Transp. Porous Media **84**, 109 (2010).
[17]A. Medina, C. Pérez-Rosales, A. Pineda, and F. J. Higuera, Rev. Mex. Fis. **47**, 537 (2001).
[18]S. Mendez, E. M. Fenton, G. R. Gallegos, D. N. Petsev, S. S. Sibbett, H. A. Stone, Y. Zhang, and G. P. López, Langmuir **26**, 1380 (2010).
[19]E. Fu, S. A. Ramsey, P. Kauffman, B. Lutz, and P. Yager, Microfluid Nanofluid. **10**, 29 (2011).
[20]A. Martinez, S. Phillips, M. Butte, and G. Whitesides, Angew. Chem., Int. Ed. **46**, 1318 (2007).
[21]A. W. Martinez, S. T. Phillips, and G. M. Whitesides, Proc. Natl. Acad. Sci. U.S.A. **105**, 19606 (2008).
[22]A. W. Martinez, S. T. Phillips, G. M. Whitesides, and E. Carrilho, Anal. Chem. **82**, 3 (2010).
[23]R. Derda, A. Laromaine, A. Mammoto, S. K. Y. Tang, T. Mammoto, D. E. Ingber, and G. M. Whitesides, Proc. Natl. Acad. Sci. U.S.A. **106**, 18457 (2009).
[24]C. Cheng, A. W. Martinez, J. Gong, C. R. Mace, S. T. Phillips, E. Carrilho, K. A. Mirka, and G. M. Whitesides, Angew. Chem., Int. Ed. **49**, 4771 (2010).

[25]Z. Nie, C. A. Nijhuis, J. Gong, X. Chen, A. Kumachev, A. W. Martinez, M. Narovlyansky, and G. M. Whitesides, Lab Chip **10**, 477 (2010).
[26]D. A. Bruzewicz, M. Reches, and G. M. Whitesides, Anal. Chem. **80**, 3387 (2008).
[27]A. W. Martinez, S. T. Phillips, B. J. Wiley, M. Gupta, and G. M. Whitesides, Lab Chip **8**, 2146 (2008).
[28]E. Carrilho, A. W. Martinez, and G. M. Whitesides, Anal. Chem. **81**, 7091 (2009).
[29]X. Li, D. R. Ballerini, and W. Shen, Biomicrofluidics **6**, 011301 (2012).
[30]T. Songjaroen, W. Dungchai, O. Chailapakul, C. S. Henry, and W. Laiwattanapaisal, Lab Chip **12**, 3392 (2012).
[31]J. Greer, S. O. Sundberg, C. T. Wittwer, and B. K. Gale, J. Micromech. Microeng. **17**, 2407 (2007).
[32]See supplementary material at http://dx.doi.org/10.1063/1.4790819 for the detailed fabrication process; the approximation of total pressure P_1 and outlet port pressure P_2; the approximation of P_3 in a paper pump; details of the theoretical calculation measurement; methods for pumping volume.
[33]J. Berthier and J. Ramsden, *Micro-Drops and Digital Microfluidics* (William Andrew Publishing, Norwich, NY, 2008), pp. 7–73.
[34]A. Borhan and K. K. Rungta, J. Colloid Interface Sci. **158**, 403 (1993).
[35]Harvard Apparatus, *Harvard Apparatus Pumps Catalog* (Harvard Apparatus, Holliston, Massachusetts, 2013), p. 13.
[36]Thermo Scientific, *Good Laboratory Pipetting Guide* (Thermo Scientific, 2010), p. 21.
[37]Harvard Apparatus, *Harvard Apparatus Pumps Catalog* (Harvard Apparatus, Holliston, Massachusetts, 2012), p. 4.
[38]M. M. Gong, B. D. MacDonald, T. V. Nguyen, and D. Sinton, Biomicrofluidics **6**, 044102 (2012).
[39]Harvard Apparatus, *Pump 11 Elite & Pump 11 Pico Plus Elite User's Manual* (Harvard Apparatus, Holliston, Massachusetts, 2012), p. 8.
[40]R. Burton-Opitz and R. Dinegar, Am. J. Physiol. **47**, 220 (1918).
[41]R. Rosencranz and S. A. Bogen, Am. J. Clin. Pathol. **125**(Suppl 1), S78 (2006).
[42]E. W. Merrill, Physiol Rev. **49**, 863 (1969).
[43]D. M. Eckmann, S. Bowers, M. Stecker, and A. T. Cheung, Anesth. Analg. **91**, 539 (2000).
[44]Z. Xu, C. Zhong, Y. Guan, X. Chen, J. Wang, and Z. Fang, Lab Chip **8**, 1658 (2008).
[45]J. Wang, H. Ahmad, C. Ma, Q. Shi, O. Vermesh, U. Vermesh, and J. Heath, Lab Chip **10**, 3157 (2010).
[46]I. Meyvantsson, J. W. Warrick, S. Hayes, A. Skoien, and D. J. Beebe, Lab Chip **8**, 717 (2008).